ChemistrySelect

ChemistrySelect
Chemistry Europe
European Chemical Societies Publishing

RESEARCH ARTICLE

Electrochemical Sensor for ATP Detection Based on Bio-Recognition of ZIF-90

Jun Zhang | Wenzhu Jiang | Bingqi Li | Zhiping Xu | Lin Zhang

Shenyang Key Laboratory of Medical Molecular Theranostic Probes in School of Pharmacy, Shenyang Medical College, Shenyang, China

Correspondence: Lin Zhang (zl210503@163.com)

Received: 26 June 2025 | **Revised:** 17 October 2025 | **Accepted:** 18 November 2025

Keywords: atp | electrochemical sensor | metal-organic framework | zif-90

ABSTRACT

Precise screening of ATP has become an issue of paramount significance for biochemical research and clinical diagnosis. Herein, a facile electrochemical sensing strategy was developed based on the one-step hydrothermal synthesis method of ALP-encapsulated MOFs (ALP@ZIF-90) composites using zeolitic imidazolate framework-90 (ZIF-90) as the support to realize the sensitive detection of ATP. The controlled-release sensing system is based on the dissolution of ALP@ZIF-90 composite that can respond to ATP, resulting in the unlocking of the pore to release ALP molecules. Then, the ALP molecules triggered the hydrolysis of *p*-nitrophenol phosphate, generating a strong diffusion current. The stimulus-responsive nanoprobes can enable sensitive detection of ATP targets with an ultralow detection limit of 0.39 pM($S/N = 3$). Its practical application potential was verified by detecting ATP in serum samples with a standard addition method. The concept proposed in this work could be further extended to an accurate early diagnosis of tumors and demonstrates significant potential for the detection of future biomarkers.

1 | Introduction

Adenosine triphosphate (ATP), composed of adenosine and three phosphate groups, can serve as the direct source of energy required for life activities [1–3]. Monitoring ATP provides important information for disease prevention and chronic disease treatment, which can effectively reduce the occurrence of diseases and increase the cure rate of patients. Detecting abnormal ATP concentration is distinctly important for a series of diseases such as hypertension, cardiovascular diseases, Parkinson's syndrome, and inflammation [4–8]. It is thus of great reference value to detect ATP for biochemical research and clinical diagnosis [9–11]. The usual analytical methods for ATP include mass spectrometry (MS), high-performance liquid chromatography (HPLC), and enzyme-linked immunosorbent assay (ELISA) [12–14]. However, these traditional methods commonly involve complicated pretreatments, expensive instrumentation, and time-consuming operations, which hardly meet the requirements of the detection sensitivity. More importantly, it is difficult to distinguish ATP from analogs such as CTP, which may eventually influence the results [15, 16]. Undoubtedly, it needs more focus to establish a rapid and sensitive method for the detection of ATP.

Metal-organic frameworks (MOFs), a class of crystalline porous materials composed of metal ions and organic ligands, have attracted researchers' attention. Compared with other materials, they are given the properties of large specific surface area, abundant metal active sites, and convenient modification [17–21]. These properties make MOFs suitable for various fields such as separation, gas adsorption, energy storage, and catalysis [22–24]. It cannot be ignored that the structural properties of MOFs contribute to the sensitivity of MOF-based electrochemical sensors. As is well known, the pore environment is an important factor affecting the mass transfer rate of the substrate and has a decisive effect on the sensitivity of sensors [25–28]. The large specific surface area makes it possible to increase the contact

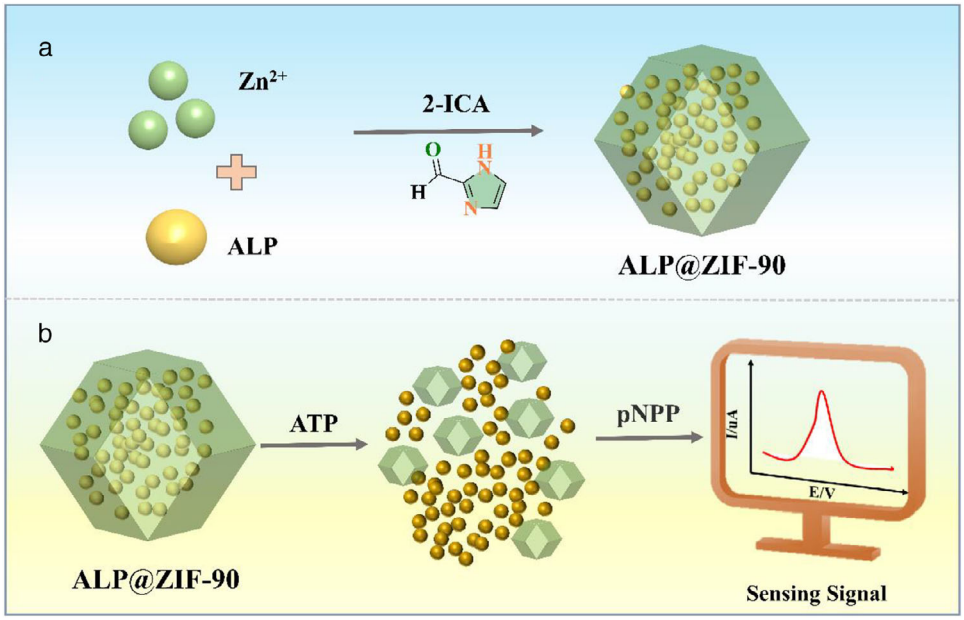

SCHEME 1 | Schematic illustration of **ALP@ZIF-90** development and its application for ATP bioanalysis.

probability between analytes and the active sites, leading to the enhancement of the sensing signal and improving sensor performance. Meanwhile, the large pore volumes are of great importance to load a large number of molecules, which is a significant factor concerning the rate of mass transfer and is decisive for detection sensitivity. Consequently, the following characteristics of MOFs make them ideal carriers to load small molecules, enzymes, and other nanomaterials for biosensing [29–32]. For example, Xie et al. reported Fe-MIL-88 as a carrier for loading hemin and glucose oxidase, achieving a cascade catalysis for thrombin detection with a low detection limit of 0.068 pM [33]. Au nanoparticle@ZIF-8(NiPd) with intrinsic peroxidase-like activity was used as a signal probe and promising nanocarriers for biomarker detection by Zhang et al., achieving a catalysis for H_2O_2 reduction with a low detection limit of 15 fM [34]. Furthermore, MOFs can serve as potent carriers to accommodate guest molecules, which can then be released controllably through external unique physical and chemical stimuli. For instance, ZIF-90 is a type of MOF formed by self-assembly of Zn^{2+} and imidazole acid-2-carboxylic acid (2-ICA) [35]. By taking advantage of its responsiveness to ATP, the ZIF-90 degrades due to the competitive coordination between ATP and Zn^{2+} of nanoparticles [36, 37]. Therefore, encapsulation of ZIF-90 and stimulus-responsive release of guest molecules have become a promising strategy in the construction of an ATP biosensing system.

Inspired by these, a sensitive and reusable electrochemical biosensing platform was designed for monitoring ATP, relying on combining ATP-responsive material with catalytic hydrolysis of ALP. Herein, a one-pot self-assembly method was employed to encapsulate phosphatase (ALP) into ZIF-90 to form ALP@ZIF-90 composites. The as-prepared **ALP@ZIF-90** nanoparticles were directly employed for the construction of the ATP sensing system, where ZIF-90 was employed to enable selective ATP recognition. When ALP was introduced, the competitive synergistic effect of ATP and Zn^{2+} led to the decomposition of ZIF-90 (Scheme 1). Therefore, the hydrolysis activity of ALP was reactivated, further catalyzing *p*-nitrophenol phosphate (*p*-NPP) to form the electroactive *p*-nitrophenol [38]. The concentration of ATP can be directly quantified by monitoring the electrochemical signal of *p*-nitrophenol without extra recognition and amplification elements. Based on this strategy, the electrochemical biosensing platform exhibits a wide linear range of 1×10^{-12}–1×10^{-5} M with a low limit of detection of 0.39 pM, which is far superior to those of the reported sensing systems. The detection of ALP in real serum samples can also be achieved, and it has an acceptable level of accuracy. The concept proposed in this work could be further extended to an accurate early diagnosis of the tumor and demonstrated significant potential for the detection of future biomarkers.

2 | Experimental Section

2.1 | Materials and Instruments

The chemicals used in this study are as follows: imidazole-2-formaldehyde (2-IAC), phosphatase (ALP), adenosine triphosphate (ATP), *p*-nitrophenol phosphate (*p*-NPP), Zn $(CH_3COO)_2$, adenosine diphosphate (ADP), adenosine monophosphate (AMP), bovine serum albumin (BSA) and glucose were purchased from Shanghai Macklin Biochemical Technology (Shanghai, China). *N*, *N*-Dimethylformamide (DMF), HCl, and NaOH were obtained from Sinopharm Chemical Reagent Co., Ltd. (Shanghai, China).

All chemical reagents were of analytical grade and used as received without further purification. In these experiments, phosphate-buffered saline (0.1 M PBS, pH 9.0) was employed as the working buffer. Doubly distilled water was used throughout the work.

The morphology of the as-prepared sample was characterized by transmission electron microscopy (TEM, JEM-F200, Japan).

Powder X-ray diffraction (PXRD) patterns were conducted on a Germany Bruker D8 Advance X-ray powder diffractometer using Cu Kα radiation (λ = 1.5418 Å). Fourier transform IR (FT-IR) spectra were recorded in the range of 4000–500 cm^{-1} using KBr pellets on a Bruker Vertex 70 FI-IR (Germany). Differential pulse voltammetry (DPV) measurements were performed on a CHI660E electrochemical workstation (Shanghai Chen Hua Instrument, China) by using a platinum wire as the counter electrode, a saturated calomel electrode (SCE) as the reference electrode, and the modified glassy carbon electrode (GCE, $\Phi = 3$ mm) as the working electrode.

2.2 | The Preparation of ZIF-90

ZIF-90 was synthesized on the basis of a previously reported method with minor modifications [39]. Briefly, 48.1 mg of 2-ICA in 10.0 mL DMF was vigorously stirred for 15 min. Thereafter, 54.8 mg of Zn $(CH_3COO)_2$ in 5.0 mL DMF was slowly added to the solution, and the final solution was stirred continuously for 15 min. The obtained products were washed with DMF and ultrapure water via centrifugation (10,000 rpm, 5 min). Finally, the obtained nanoparticles were dispersed in ultrapure water (2 mg mL^{-1}). Yield: 59.5% (based on Zn^{2+}).

2.3 | The Preparation of ALP @ZIF-90

ALP @ZIF-90 was synthesized on basis of a previously reported method with minor modifications [40]. To fabricate ALP@ZIF-90, 5 mL of 1 mg mL^{-1}ALP was added to 1 mL of 0.1 mol L^{-1} 2-IAC with continuous stirring, and then Zn $(CH_3COOH)_2$ was added to the mixture, which was stirred for 15 min in an ice bath. Following that, the ALP@ZIF-90 products were washed three times via low-temperature centrifugation and dispersed in ultrapure water. Finally, the prepared composites were washed with sodium dodecyl sulfonate to remove unencapsulated enzyme from the solution and yield pure ALP@ZIF-90 nanocomposites. (2 mg mL^{-1}). Yield: 49.5% (based on Zn^{2+}).

2.4 | Detection of ATP

The fabrication process of the electrochemical biosensor involved three steps. First, 2 mL of varying concentrations of ATP (1×10^{-12}, 1×10^{-11}, 1×10^{-10}, 1×10^{-9}, 1×10^{-8}, 1×10^{-7}, 1×10^{-6} M, 1×10^{-5} M) were added to the 1 mL ALP@ZIF-90 solution and allowed to incubate for 5 min. After centrifugation at 10000 rpm, 2 mL of 1.0 mM *p*-NPP solution was added to the above solution and incubated at room temperature for 10 min. Ultimately, the supernatant was exposed to DPV measurement.

3 | Results and Discussion

3.1 | Principle of the Electrochemical Modification Method

The as-prepared ALP@ZIF-90 nanoparticles were directly employed for the construction of an ATP sensing system, where ZIF-90 served as a host. As illustrated in Scheme 1, this sensing system also contained ATP as the recognition component. Once the target analyte, ATP, was introduced into the solution, it decomposed ZIF-90 due to the fact that the phosphate group and adenosine group in ATP have stronger coordination with Zn^{2+} than the iminazole group in 2-ICA, leading to the breakdown of ALP@ZIF-90 nanoparticles. Then, the ALP molecules would be released and further trigger the hydrolysis of *p*-NPP, generating a strong diffusion current. On the contrary, in the absence of ATP, because of the electrical insulation of ZIF-90, the "locked" ATP molecules in the ALP@ZIF-90 composites produced a very weak electrochemical signal. Based on the ATP-responsive MOFs composites, the electrochemical determination of ATP with good selectivity, sensitivity, and anti-interference ability was readily achieved.

3.2 | Characterization of Synthesized ALP @ZIF-90

The ALP @ZIF-90 nanoparticles were obtained through a one-step reaction, which introduced ALP to $Zn^{2+}$and 2-ICA mixed solution. The structure and morphology of ZIF-90 and ALP @ZIF-90 nanoparticles were characterized by PXRD, TEM, and FT-IR. X-ray diffraction (XRD) characterizations were shown in Figure 1a; the diffraction peaks match well with the prepared ZIF-90 and simulated pure ZIF-90, implying the successful preparation of ALP@ZIF-90. Moreover, the XRD peaks of ALP in the pattern of ALP@ZIF-90 were not observed, further proving that ALP was wrapped inside the ZIF-90 rather than physically adsorbed on its surface. In addition, from the FT-IR spectra, in comparison to ZIF-90, ALP@ZIF-90 displayed new peaks at 1029 and 789 cm^{-1}, which were attributable to ALP. All of the above adequately proved the successful preparation of ALP @ZIF-90. TEM and energy-dispersive X-ray spectrometer (EDS) were used for further characterization. As shown in Figure 2b,c, the obtained ZIF-90 and ALP @ZIF-90 showed a uniformly dispersed structure with an average diameter of 100 nm. Moreover, the N, Zn, C, and O elements were uniformly distributed in the ALP @ZIF-90 nanoparticles (Figure 2d). The above obtained results indicated that ALP molecules were successfully encapsulated in the framework of ZIF-90, and exhibit promising potential for application in the determination of ATP.

3.3 | Optimization of Detection Conditions

To establish the validity of the MOFs-based homogeneous electrochemical strategy, DPV responses of the ALP@ZIF-90 composites under different experimental conditions were monitored and shown in Figure 3. Because the amount of ALP directly affected the DPV signals, we investigated the incubation time of ATP. As shown in Figure 3a, the DPV signals rose with increasing incubation time, demonstrating that more ALP molecules can be released from the pores of ZIF-90. When the incubation time was extended from 5 to 7 min, the DPV signals leveled off. So, 5 min was utilized as the optimal incubation time of ATP. Another important aspect to be investigated was the concentration of *p*-NPP, seven different *p*-NPP concentrations (0.2, 0.4, 0.6, 0.8, 1.0, 1.2, and 1.4 mM) were studied. From Figure 3b, the peak current rose significantly as the *p*-NPP concentration increased from 0.2 to 1.0 mM. Subsequently, the

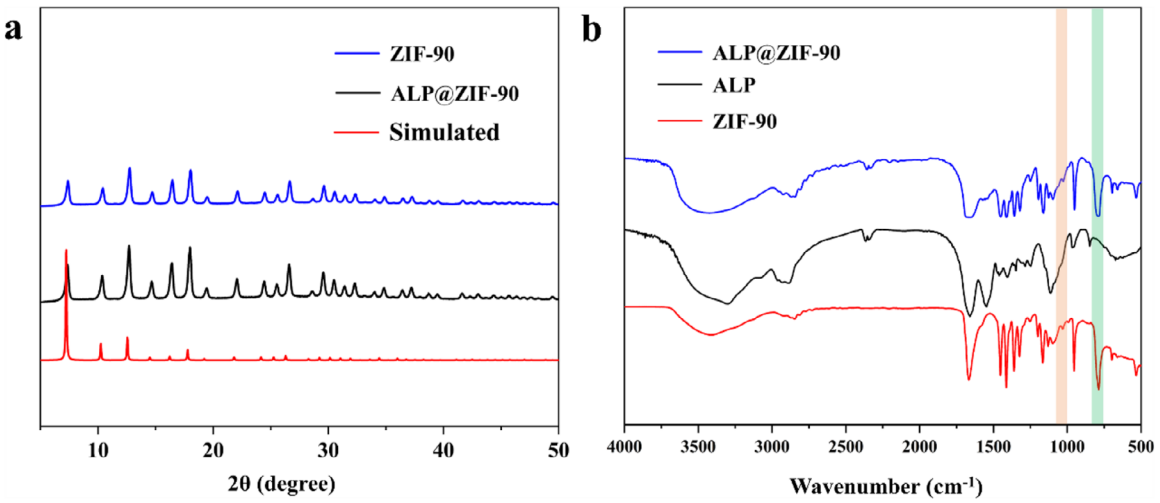

FIGURE 1 | PXRD patterns (a) and FT-IR spectra (b) of ZIF-90 and ALP@ZIF-90.

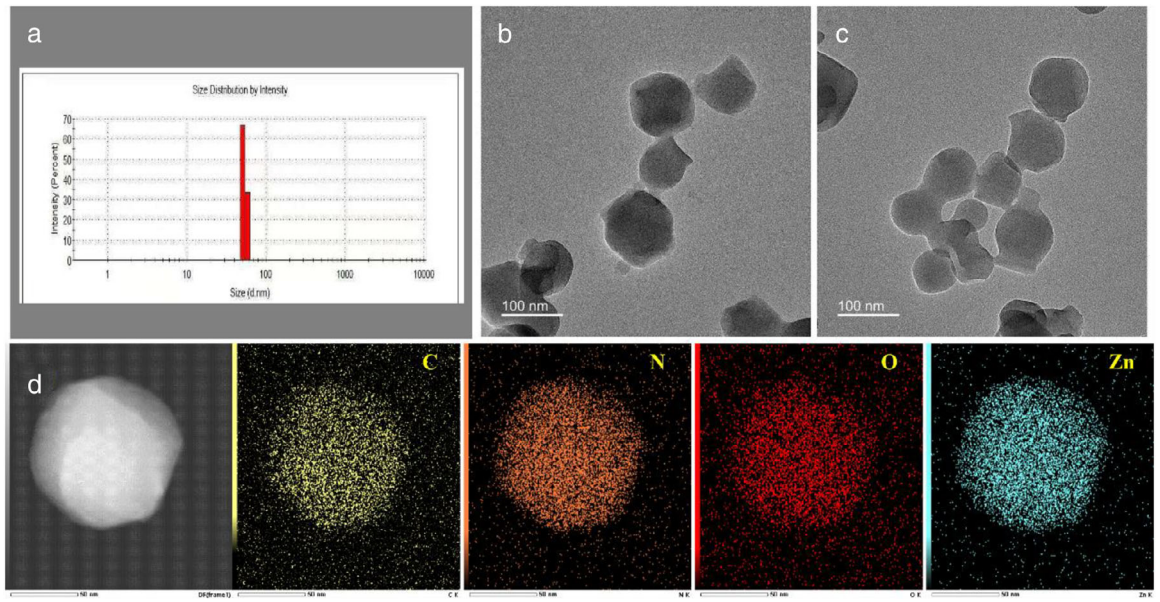

FIGURE 2 | Particle size distribution diagram of ZIF-90 (a) TEM images of ZIF-90 (b) and ALP@ZIF-90 samples (c). EDS mapping images of ALP@ZIF-90 and the corresponding distribution of C, N, O, and Zn elements (d).

addition of *p*-NPP from 1.0 to 1.4 mM caused the peak current to gradually decrease. Therefore, 1.0 mM was set as the optimal *p*-NPP concentration. Optimization of the reaction time of ALP catalysis is shown in Figure 3c. By comparing the strength of the peak signal, it was found that the peak current remarkably increased with the reaction time increased from 5 to 10 min, and then stabilized after 10 min, probably because the ALP incubation was almost completed at 10 min. Accordingly, 10 min was chosen as the best reaction time of ALP catalysis for further testing. Additionally, the pH of the buffer is essential to evaluate the sensitivity of the biosensors as the bioactivity of the ALP depends on the pH of the solution. Figure 3d showed the relationship between the DPV currents with the pH of PBS from 5 to 10, the largest response current was obtained at pH 9. Hence, an optimum pH of 9 was adopted for the following experiments. Eventually, 5 min ATP incubation time, 1.0 mM of *p*-NPP concentration, 10 min ALP catalysis time, and pH 9.0 of PBS substrate were determined to be the optimal parameters for sensing experiments.

3.4 | Analytical Performance of Constructed ATP Biosensor

Temperature directly dominates the catalytic activity of ALP, affects the sensing signal production, and further decides the detection limit and performance of the sensor. Before testing, the relationship between inhibition effect and incubation temperature of ALP was explored. From Figure S1, the response rapidly enhanced with the incubation time was increased to 37°C, then the peak current levels off, suggesting that 37°C is the optimum incubation temperature. Under the optimized conditions, the effect of ATP on the analytical response of the assembled biosensor is examined by DPV. As shown in Figure 4a,

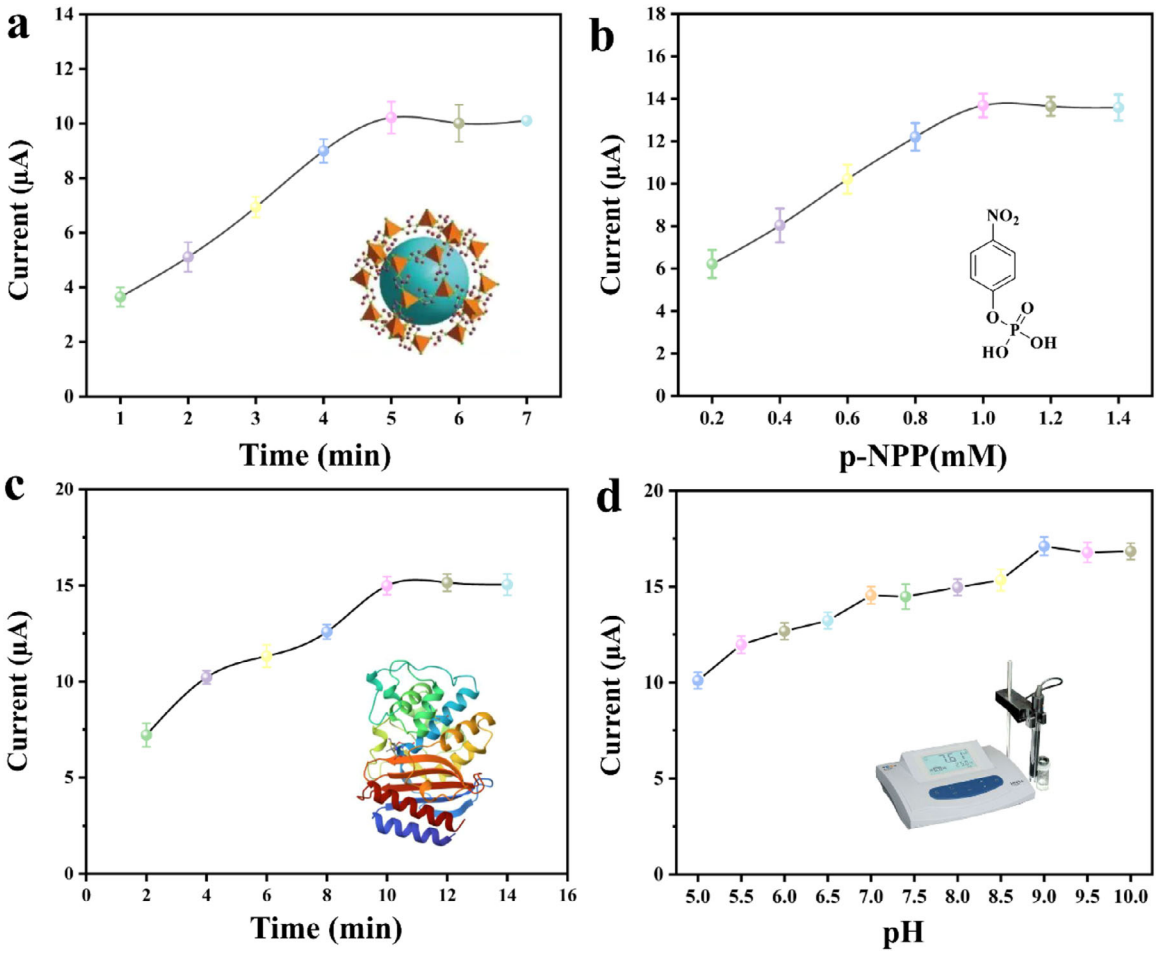

FIGURE 3 | Effects of (a) incubation time of ATP, (b) p-NPP concentration, (c) reaction time of ALP catalysis and (d) pH on the DPV responses.

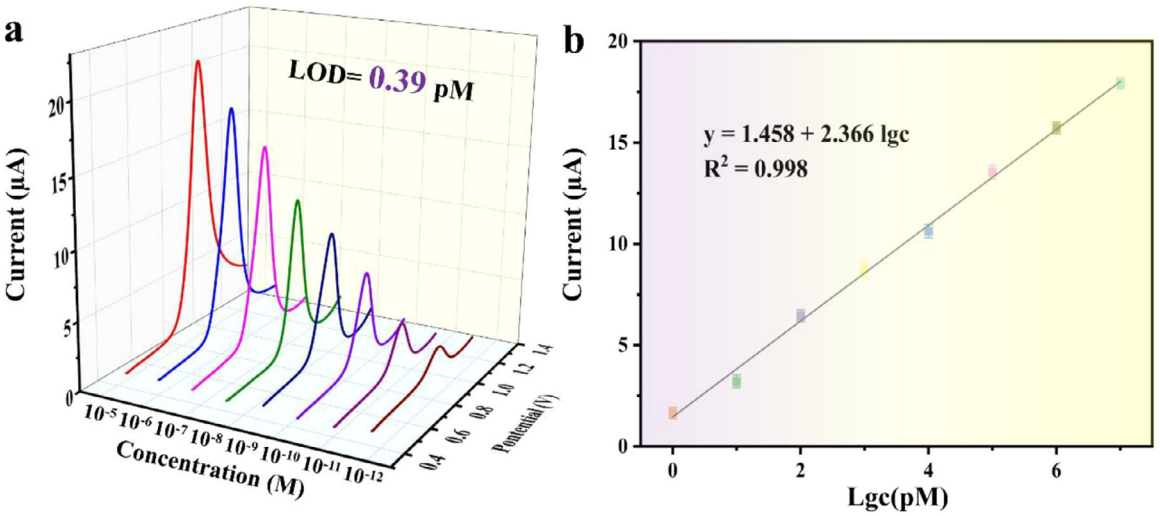

FIGURE 4 | (a) DPV responses of the sensor to different concentrations of ATP, (b) The corresponding calibration plot for ATP detection.

the oxidation peak current signals at about 0.9 V increased successively with increasing the concentration of ATP from 1×10^{-12} to 1×10^{-5} M, which could be attributed to the sensing principle that more target ATP triggered the release of more ALP. Obviously, the proposed ATP sensor exhibited outstanding electrochemical sensitivity. As can be seen from Figure 4b, a good linear dependence between the peak current and the logarithm of ATP concentration (lgc) is obtained with a low detection of 0.39 pM according to the 3σ rule, and the equation for the linear regression was $y = 2.366$ lgc + 1.458 ($R^2 = 0.998$). According to

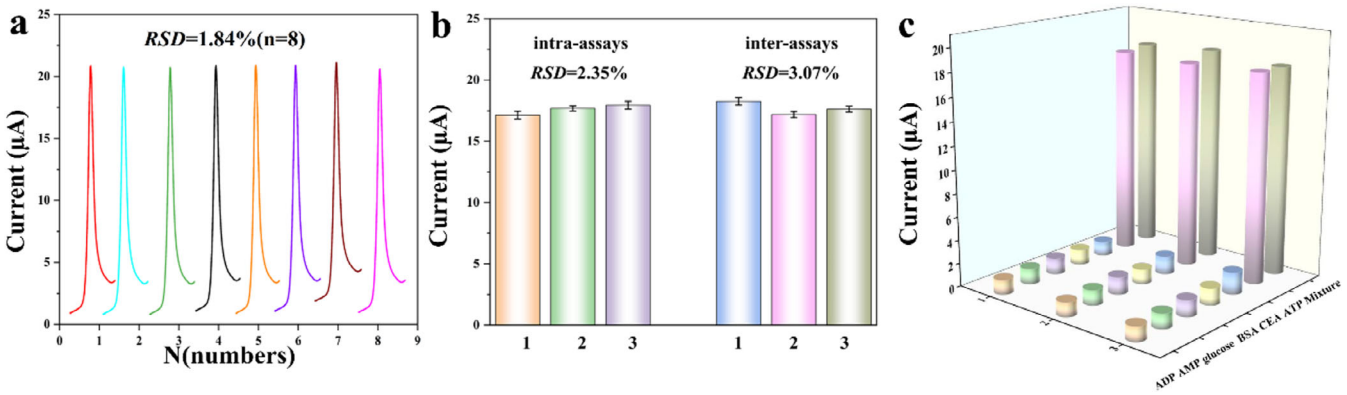

FIGURE 5 | (a) Stability test of the developed biosensor incubated with 10^{-5} M ATP for intermittent DPV scanning ($n = 8$), (b) Reproducibility of the proposed biosensor incubated with 10^{-5} M ATP, (c) DPV responses of the sensing system with the interfering substances (10^{-4} M).

the comparison with reported electrochemical detection or other methods compared with the obtained sensor in Table S1, the proposed biosensor exhibited promising detection performance with a satisfactory LOD and a favorable linear range. The high performance may result from ZIF-90's porous structure and one-step preparation strategy, increasing the loading of ALP. More exactly, the strong ability to recognize ATP could increase the concentration of released ALP when only a small amount of ATP is added.

Overall, this ALP@ZIF-90-based biosensor possessed apparent advantages of simple operation, fast analysis, and low price, and therefore it was regarded as a more popular tool for ultrasensitive analysis of ATP, favoring the rapid, early, and accurate diagnosis of ATP-related diseases.

3.5 | Stability, Reproducibility, and Selectivity of Proposed ATP Biosensor

For the study of the stability of the proposed biosensor, the sensing platform was checked under consecutive DPV tests for 8 times for intermittent DPV scanning after being treated with 10^{-5} M ATP. As shown in Figure 5a, the DPV response remains stable at about 17 μA with a relative standard deviation (*RSD*) of 1.84%, suggesting an excellent operational stability of the MOF-based biosensor. Moreover, six different ALP@ZIF-90 biosensors were prepared using the same process. The current responses of the biosensor were recorded in 0.1 M PBS (pH = 9.0) towards 1×10^{-5} M ATP after being treated with 2 mL 1.0 mM *p*-NPP solution. The *RSD* of intra and inter-assays are found to be 2.35% and 3.07%, respectively, indicating a desirable reproducibility of the proposed biosensor (Figure 5b).

Selectivity study is another requisite criterion for actual sample detection. To further study the stability, a range of common interfering substances in the actual sample detection, including ADP, AMP, glucose, BSA, and CEA, were evaluated. The concentration of ATP was 1×10^{-5} M, and the concentration of all these interferences was 1×10^{-4} M. As illustrated in Figure 5c, in the presence of ATP, the electrochemical signal with the interfering substances exhibited a very limited response compared with ATP alone. Furthermore, the intensity of the sensor was almost unchanged after the addition of interfering substances coexisting with ATP, indicating that the above substances have little effect on the detection of ATP. Besides, metal ions, including Co^{2+}, Ni^{2+}, Fe^{2+}, Mn^{2+}, Zn^{2+}, and K^{+}, were employed to check the sensing performance of the as-synthesized biosensor. In the presence of ATP, the biosensor system with metal ions showed a negligible current change when compared to ATP (Figure S2). Moreover, when ATP and all the interferences were mixed in the solution, the DPV current responses were almost identical to those from only ATP. The results demonstrated that the possible interfering substances did not cause interference in the ATP assay, and the biosensor exhibited enhanced selectivity.

TABLE 1 | Recovery tests of ATP detection in serum samples.

Samples	Added (pM)	Found (pM)	Recovery (%)	RSD (%)
1	10.00	9.91	99.10	3.24
2	100.00	97.94	97.94	2.98
3	1000.00	996.64	99.66	3.12
4	5000.00	5034.72	100.69	3.13
5	10000.00	9995.39	99.95	1.94

3.6 | ATP Determination in Serum

To validate the efficacy and precision of the proposed ATP sensor for real sample analysis, different concentrations of ATP were added to real serum samples (100-fold diluted), which were provided by Shenyang Medical College. As shown in Table 1, the recoveries ranged from 97.94% to 100.69% and the *RSDs* were in the range of 1.94–3.24 for the electrochemical technique, which confirmed that the sensor demonstrates satisfactory performance and can effectively detect ATP in serum samples, demonstrating a workable application prospect of the ATP detection in clinical samples.

4 | Conclusions

In summary, this work proposed an electroanalytical method based on the one-step hydrothermal synthesis method of ALP-encapsulated MOFs composites to realize the sensitive detection of ATP. In this strategy, it is confirmed that the composites could be easily disintegrated in the presence of ATP, which consequently contributed to the release of numerous ALP molecules for generating detectable electrochemical signals.

The ALP@ZIF-90-based sensing system has the advantages of simple preparation, high stability, rapid response to the target, and good selectivity, which exhibits a wide linear range of 1×10^{-12}–1×10^{-5} M and a very low detection limit of 0.39 pM, far superior to those of the reported sensing systems. Moreover, this strategy was also successfully applied for ATP determination in real samples, demonstrating a promising prospect in clinical diagnosis.

Acknowledgments

The authors appreciate financial support from Joint Project supported by the Natural Science Foundation of Science and Technology Department of Liaoning Province (2023-BSBA-296, 2024-MSLH-451), Science and Technology Research Project of Liaoning Education Department (No. JYTMS20231405), Basic Scientific Research Project for Universities of Liaoning Education Department (LJ212510164028).

Conflicts of Interest

The authors declare no conflicts of interest.

Data Availability Statement

The data that support the findings of this study are available from the corresponding author upon reasonable request.

References

1. H. Kang, S. Oka, D. Y. Lee, et al., "Sirt1 Carboxyl-Domain is an ATP-Repressible Domain That is Transferrable to Other Proteins," *Nature Communications* 8 (2017): 15560.

2. Z. Ning, Y. Zheng, D. Pan, Y. Zhang, and Y. Shen, "Coupling Aptazyme and Catalytic Hairpin Assembly for Cascaded Dual Signal Amplified Electrochemiluminescence Biosensing," *Biosensors and Bioelectronics* 150 (2020): 111945, https://doi.org/10.1016/j.bios.2019.111945.

3. S. Shrivastava, T. Q. Trung, and N. E. Lee, "Recent Progress, Challenges, and Prospects of Fully Integrated Mobile and Wearable Point-of-Care Testing Systems for Self-Testing," *Chemical Society Reviews* 49 (2020): 1812–1866, https://doi.org/10.1039/C9CS00319C.

4. B. Ebanks, T. L. Ingram, and L. Chakrabarti, "ATP Synthase and Alzheimer's Disease: Putting a Spin on the Mitochondrial Hypothesis," *Aging* 12, no. 16 (2020): 16647–16662, https://doi.org/10.18632/aging.103867.

5. I. S. Schädlich, R. Winzer, J. Stabernack, E. Tolosa, T. Magnus, and B. Rissiek, "The Role of the ATP-Adenosine Axis in Ischemic Stroke," *Seminars in Immunopathology* 45, no. 3 (2023): 347–365, https://doi.org/10.1007/s00281-023-00987-3.

6. Y. Huang, D. Hu, C. Huang, and C. G. Nichols, "Genetic Discovery of ATP-Sensitive K+ Channels in Cardiovascular Diseases," *Circulation: Arrhythmia and Electrophysiology* 12, no. 5 (2019): 007322.

7. M. Nakano, H. Imamura, N. Sasaoka, et al., "ATP Maintenance via Two Types of ATP Regulators Mitigates Pathological Phenotypes in Mouse Models of Parkinson's Disease," *EBioMedicine* 22 (2017): 225–241.

8. A. V. Gourine, E. Llaudet, N. Dale, and K. M. Spyer, "ATP is a Mediator of Chemosensory Transduction in the Central Nervous System," *Nature* 436, no. 7047 (2005): 108–111, https://doi.org/10.1038/nature03690.

9. W. Shen, X. Lin, C. Y. Jiang, et al., "Reliable Quantitative SERS Analysis Facilitated by Core–Shell Nanoparticles With Embedded Internal Standards," *Angewandte Chemie International Edition* 54, no. 25 (2015): 7308–7312, https://doi.org/10.1002/anie.201502171.

10. M. J. Li, Y. N. Zheng, W. B. Liang, R. Yuan, and Y. Q. Chai, "Using *p*-Type PbS Quantum Dots to Quench Photocurrent of Fullerene–Au NP@MoS 2 Composite Structure for Ultrasensitive Photoelectrochemical Detection of ATP," *American Chemical Society Applied Materials and Interfaces* 9 (2017): 42111–42120, https://doi.org/10.1021/acsami.7b13894.

11. S. Li, X. Zhao, X. Yu, et al., "Fe 3 O 4 Nanozymes With Aptamer-Tuned Catalysis for Selective Colorimetric Analysis of ATP in Blood," *Analytical Chemistry* 91 (2019): 14737–14742, https://doi.org/10.1021/acs.analchem.9b04116.

12. M. V. Zamaraeva, R. Z. Sabirov, E. Maeno, Y. Ando-Akatsuka, S. V. Bessonova, and Y. Okada, "Cells Die With Increased Cytosolic ATP During Apoptosis: A Bioluminescence Study With Intracellular Luciferase," *Cell Death and Differentiation* 12, no. 11 (2005): 1390–1397, https://doi.org/10.1038/sj.cdd.4401661.

13. P. Herijgers, K. Overloop, Y. Toshima, et al., "Ischaemic ATP Degradation Studied by HPLC and31P-NMR Spectroscopy: Do the Two Techniques Observe the Same ATP Pools?," *Basic Research in Cardiology* 89 (1994): 50–60, https://doi.org/10.1007/BF00788677.

14. M. Rajendran, E. Dane, J. Conley, and M. tantama, "Imaging Adenosine Triphosphate (ATP)," *Biological Bulletin* 231 (2016): 73–84, https://doi.org/10.1086/689592.

15. X. He, X. Zhao, W. Deng, Y. Tan, and Q. Xie, "CdSe Quantum Dots-Decorated ZnIn2S4 Nanosheets for "Signal-On" Photoelectrochemical Aptasensing of ATP by Integrating Exciton Energy Transfer With Exciton-Plasmon Coupling," *Sensors and Actuators B: Chemical* 348 (2021): 130686, https://doi.org/10.1016/j.snb.2021.130686.

16. W. Liu, X. Zhu, M. Mozneb, L. Nagahara, and T. Y. Hu, "Lighting up ATP in Cells and Tissues Using a Simple Aptamer-Based Fluorescent Probe," *Microchimica Acta* 188 (2021): 352.

17. Y. J. Cui, Y. F. Yue, G. D. Qian, and B. L. Chen, "Luminescent Functional Metal–Organic Frameworks," *Chemical Reviews* 112 (2012): 1126–1162, https://doi.org/10.1021/cr200101d.

18. J. R. Li, R. J. Kuppler, and H. C. Zhou, "Selective Gas Adsorption and Separation in Metal–Organic Frameworks," *Chemical Society Reviews* 38 (2009): 1477–1504, https://doi.org/10.1039/b802426j.

19. L. X. Su, H. Wu, S. K. Zhang, C. X. Cui, S. N. Zhou, and H. Pang, "Insight Into Intermediate Behaviors and Design Strategies of Platinum Group Metal-Based Alkaline Hydrogen Oxidation Catalysts," *Advanced Materials* 37, no. 4 (2025): 2414628, https://doi.org/10.1002/adma.202414628.

20. L. X. Su, S. K. Zhang, H. Wu, S. N. Zhou, C. X. Cui, and H. Pang, "Mechanism Insights and Design Strategies for Metal-Organic Framework-Based Alkaline Hydrogen Evolution Reaction Electrocatalysts," *Nano Energy* 130 (2024): 110177, https://doi.org/10.1016/j.nanoen.2024.110177.

21. L. X. Su, S. N. Zhou, C. X. Cui, S. K. Zhang, H. Wu, and H. Pang, "*p*-Block Element in Platinum Group Metal: Mechanism Insight and Structure Design for Alkaline Hydrogen Electrocatalysis," *Nano Research* 18, no. 6 (2025): 94907442, https://doi.org/10.26599/NR.2025.94907442.

22. O. Changhwan, A. Nandy, S. W. Yue, and H. J. Kulik, "MOFs With the Stability for Practical Gas Adsorption Applications Require New Design Rules," *American Chemical Society Applied Materials and Interfaces* 16 (2024): 55541–55554.

23. A. Chaouiki, M. Chafiq, R. Salghi, et al., "Versatile Integration of MOF and MXene Composites for Next-Generation Hybrid Energy Storage Solutions," *Journal of Energy Chemistry* 104 (2025): 687–715, https://doi.org/10.1016/j.jechem.2025.01.012.

24. S. Wang, W. S. Liu, J. Wang, et al., "Mechanochemical Encapsulation of Enzymes into MOFs for Photoenzymatic Enantioselective Catalysis,"*American Chemical Society Materials Letters* 6, (2024): 2609–2616, http://doi.org.10.1021/acsmaterialslett.4c00629.

25. B. Mohan, "Tuned Porous MOFs & COFs for Arsenic Removal-Advanced Water Remediation Approach," *Desalination* 592 (2024): 118075, https://doi.org/10.1016/j.desal.2024.118075.

26. B. Mohan, M. B. Asif, and A. J. L. Pombeiro, "Engineered Conductive Metal–Organic Frameworks for Electrochemical Detection of Urinary Biomarkers," *Small* 21 (2025): 2406222, https://doi.org/10.1002/smll.202406222.

27. B. Mohan, S. Ručman, P. Singjai, et al., "Advanced Electrochemiluminescent Approaches for Contaminant Detection in Food Matrices Using Metal-Organic Framework Composites," *Food Chemistry* 470 (2025): 142625, https://doi.org/10.1016/j.foodchem.2024.142625.

28. L. S. Wang, X. Q. Li, B. L. Wang, et al., "Garnering Sensitivity: A Horseradish Peroxidase and MoS2@Black Phosphorene Based Electrochemical Biosensor for Glyphosate Detection," *Bioelectrochemistry* 165 (2025): 108991, https://doi.org/10.1016/j.bioelechem.2025.108991.

29. J. F. Chang, W. Lv, X. Li, Q. Li, and H. Y. Li, "One-Step Synthesis of Methylene Blue-Encapsulated Zeolitic Imidazolate Framework for Dual-Signal Fluorescent and Homogeneous Electrochemical Biosensing," *Analytical Chemistry* 92 (2020): 8959–8964, https://doi.org/10.1021/acs.analchem.0c00952.

30. S. Wu, C. Li, H. Shi, Y. Huang, and G. X. Li, "Design of Metal–Organic Framework-Based Nanoprobes for Multicolor Detection of DNA Targets With Improved Sensitivity," *Analytical Chemistry* 90 (2018): 9929–9935.

31. X. L. Zhou, Z. Y. Shao, S. H. Yan, et al., "Coencapsulating TMB Probes and Bimetallic MOF Nanozymes in a Hydrogel Patch for Fabricating Reusable Visual VC Sensors," *Analytical Chemistry* 96, no. 43 (2024): 17310–17318, https://doi.org/10.1021/acs.analchem.4c03665.

32. Y. Huang, R. Q. Liang, H. Yu, et al., "Thi-Au-Fe3O4 Confined in ZIF-8 Nanoreactor as Signal-Amplifying Tag for Constructing High-Efficiency Electrochemical Platform," *Sensors and Actuators B: Chemical* 305 (2020): 127496, https://doi.org/10.1016/j.snb.2019.127496.

33. S. Xie, J. Ye, Y. Yuan, Y. Q. Chai, and R. Yuan, "A Multifunctional Hemin@Metal–Organic Framework and Its Application to Construct an Electrochemical Aptasensor for Thrombin Detection," *Nanoscale* 7 (2015): 18232–18238, https://doi.org/10.1039/C5NR04532K.

34. T. Zhang, Y. Song, Y. Xing, et al., "The Synergistic Effect of Au-COF Nanosheets and Artificial Peroxidase Au@ZIF-8(NiPd) Rhombic Dodecahedra for Signal Amplification for Biomarker Detection," *Nanoscale* 11 (2019): 20221–20227.

35. S. Q. Chen, H. K. Pang, J. N. Sun, and K. X. Li, "Research Advances and Applications of ZIF-90 Metal–Organic Framework Nanoparticles in the Biomedical Field," *Materials Chemistry Frontiers* 8 (2024): 1195–1211, https://doi.org/10.1039/D3QM01020A.

36. J. Deng, K. Wang, M. Wang, P. Yu, and L. Mao, "Mitochondria Targeted Nanoscale Zeolitic Imidazole Framework-90 for ATP Imaging in Live Cells," *Journal of the American Chemical Society* 139 (2017): 5877–5882, https://doi.org/10.1021/jacs.7b01229.

37. X. Yang, Q. Tang, Y. Jiang, M. Zhang, M. Wang, and L. Mao, "Nanoscale ATP-Responsive Zeolitic Imidazole Framework-90 as a General Platform for Cytosolic Protein Delivery and Genome Editing," *Journal of the American Chemical Society* 141 (2019): 3782–3786, https://doi.org/10.1021/jacs.8b11996.

38. P. J. Ni, C. X. Chen, Y. Y. Jiang, C. H. Zhang, B. Wang, and Y. Z. Lu, "A Fluorescent Assay for Alkaline Phosphatase Activity Based on Inner Filter Effect by In-Situ Formation of Fluorescent Azamonardine," *Sensors and Actuators B: Chemical* 302 (2020): 127145, https://doi.org/10.1016/j.snb.2019.127145.

39. Y. W. Wang, P. Qi, D. Zhang, Y. Zeng, Y. Sun, and P. Wang, "Dual-Signal Viscosity Flow Paper Sensor for ATP Detection Based on Bio-Recognition and Nanozyme Activity Regulation of ZIF-90," *Chemical Engineering Journal* 481 (2024): 148590, https://doi.org/10.1016/j.cej.2024.148590.

40. Y. He, C. F. Xie, Q. Y. Zhang, et al., "SERS Immunoassay Based on an Enzyme-Catalyzed Cascade Reaction and Metal–Organic Framework/Alkaline Phosphatase for Ultrasensitive Detection of Adenosine Triphosphate," *American Chemical Society Applied Materials and Interfaces* 16, no. 1 (2024): 1712–1718, https://doi.org/10.1021/acsami.3c13512.

Supporting Information

Additional supporting information can be found online in the Supporting Information section.

Supporting File: slct71987-sup-0001-SuppMat.docx